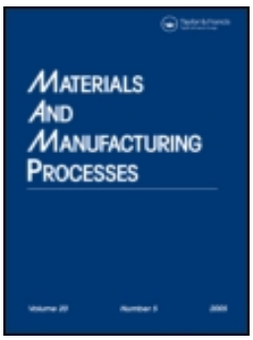

Materials and Manufacturing Processes

ISSN: 1042-6914 (Print) 1532-2475 (Online) Journal homepage: http://www.tandfonline.com/loi/lmmp20

Effects of Core Topology on Sound Insulation Performance of Lightweight All-Metallic Sandwich Panels

F. X. Xin & T. J. Lu

To cite this article: F. X. Xin & T. J. Lu (2011) Effects of Core Topology on Sound Insulation Performance of Lightweight All-Metallic Sandwich Panels, Materials and Manufacturing Processes, 26:9, 1213-1221, DOI: 10.1080/10426914.2010.531241

To link to this article: http://dx.doi.org/10.1080/10426914.2010.531241

Accepted author version posted online: 24 May 2011.
Published online: 24 May 2011.

Materials and Manufacturing Processes, 26: 1213–1221, 2011

ISSN: 1042-6914 print/1532-2475 online
DOI: 10.1080/10426914.2010.531241

Taylor & Francis
Taylor & Francis Group

Effects of Core Topology on Sound Insulation Performance of Lightweight All-Metallic Sandwich Panels

F. X. Xin and T. J. Lu

State Key Laboratory for Strength and Vibration, School of Aerospace, Xi'an Jiaotong University, Xi'an, China

An analytical study of sound transmission through all-metallic, two-dimensional, periodic sandwich structures having corrugated core is presented. The space-harmonic method is employed, and an equivalent structure containing one translational spring and one rotational spring per unit cell is proposed to simplify the analysis of the vibroacoustic problem. It is demonstrated that the core geometry exerts a significant effect on the sound insulation performance of the sandwich, so that one may tailor the core topology for specified acoustic applications. Subsequent analysis of the sound transmission loss (*STL*) and dispersion curves of the structure leads to fundamental insight into the physical mechanisms behind the appearance of various peaks and dips on the *STL* versus frequency curves. As the weight, stiffness, and acoustic property of the sandwich structures all change with the alteration of core configuration and geometry, it is further demonstrated that it is possible to explore the multifunctionality of the structure by optimally designing the core topology.

Keywords Corrugated core; Optimal design; Sandwich panel; Sound transmission loss.

Introduction

Lightweight sandwich structures comprising two facesheets and an (fluid through) open core have attractive structural load-bearing and heat-dissipation attributes [1, 2], and hence have found increasingly wide applications in high-speed transportation, aerospace and aeronautical aircrafts, ships, and other transportation vehicles where weight saving is of major concern [3–20]. Amongst these applications, an important issue is noise transmission from exterior of cabin into the interior, inasmuch as that has a particular significance for the safety and comfort of civil or military vehicles. However, to date, only a few investigations have focused on the fluid-structural coupling and dynamic responses of the sandwich structure as well as the physical mechanisms of sound transmission across the structure (see, e.g., [3, 4]).

A typical lightweight all-metallic sandwich panel is that shown in Fig. 1 which has found successful applications in modern express locomotive and ship constructions. The main attractiveness of this type of sandwich is its simple 2-dimensional (2D) corrugated core, which can be either connected to the facesheets via laser welding or formed together with the facesheets as one integral structure using the method of extrusion. In addition to carry structural loads, the openness of the corrugated core also allows the sandwich to be used as an effective heat dissipation medium, either separately or simultaneously [21, 22]. For practical applications such as express locomotives and ships, however, it is also necessary to investigate the sound insulation capability of the sandwich structure, especially the influence of core geometry on sound transmission across the structure. This task is performed in the current study. Together with load-bearing and/or heat-dissipation properties, the knowledge thus acquired on sound insulation capability would be useful for the design and manufacture of sandwich structures having corrugated cores.

Extensive investigations over the past decades have been dedicated to studying the sound insulation performances of periodic beams [24, 25], single plates [26–28], and double-panels with air cavity [29–38], or structural connections [31, 39–56]. For example, the sound transmission loss (*STL*) of a structure containing two impervious layers, an air space, and two acoustical blankets was studied by Beranek et al. [31] for normal incident sound. London [32] studied that the transmission of sound across a double wall consisting of two identical single walls coupled by an airspace by considering the impedance of a single wall, and achieved good agreement between model predictions and experimental measurements. The problem of transmission of a plane wave through two infinite parallel plates connected by periodical frames was solved by Lin and Garrelick [40], while that for an infinite sandwich panel with a constrained viscoelastic damping layer was analyzed by Narayanan and Shanbhag [50]. Takahashi [41] studied the problem of sound radiation from periodically connected (e.g., point connected, point connected with rib-stiffening, and rib-connected) infinite double-plate structures excited by a harmonic point force. Using the multiple-reflection theory, Cummings et al. [29] investigated random incidence transmission loss of a thin double aluminum panel with glass fiber absorbent around the edge of the cavity. Mathur et al. [57] investigated the *STL* through periodically stiffened panels and double-leaf structures, and proposed a theoretical model using the space-harmonic method. Lee and Kim [39] solved the vibroacoustic problem of a single stiffened plate subjected to a plane sound wave using the space-harmonic

Received April 5, 2010; Accepted May 20, 2010
Address correspondence to T. J. Lu, State Key Laboratory for Strength and Vibration, School of Aerospace, Xi'an Jiaotong University, Xi'an 710049, China; E-mail: tjlu@mail.xjtu.edu.cn

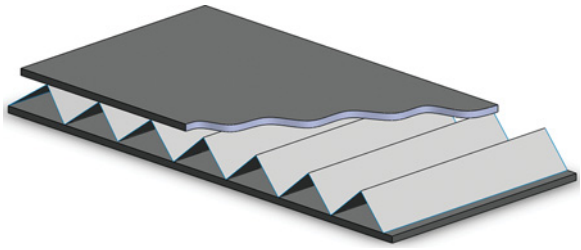

FIGURE 1.—Illustration of a typical sandwich panel with corrugated core [13, 23] (color figure available online).

approach proposed by Mead and Pujara [25]. Wang et al. [42] extended the space-harmonic approach to double-leaf partitions stiffened by periodic parallel studs, and provided detailed physical interpretations for the mechanisms of sound transmission through the structure. However, few studies have addressed the issue of sound transmission across 2D sandwich structures with corrugated core.

The purpose of the present article is to analytically study the sound insulation performance of all-metallic sandwich structure with corrugated core as shown in Fig. 1, with focus placed upon the influence of core geometry as well as the physical insight of the associated vibroacoustic phenomena. In Section 2, the theoretical development of the acoustic model is presented. Based on model predictions, the effects of core geometry on the vibroacoustic performance of the sandwich are quantified in Section 3.1. Physical interpretations of the appearances of various peaks and dips on *STL* versus frequency curves are presented in Section 3.2. Finally, the article concludes with a summary of current findings and a suggestion of future investigations required for multifunctional design of the sandwich.

DEVELOPMENT OF THEORETICAL MODEL

The transmission of sound through an infinite (in x- and z-directions) 2D sandwich panel with corrugated core is schematically illustrated in Fig. 2. A harmonic sound wave (with angular frequency ω) impinges on the left-side facesheet with incidence angle θ. Whilst part of the sound is reflected back, the remaining portion transmits into the right-side of the sandwich panel via two paths: corrugated core as structural route and air cavity as airborne route. The sandwich panel with corrugated core is modeled as two parallel plates (facesheets) structurally connected by uniformly distributed (equivalent) translational springs and rotational springs, and the mass of the core is considered as lumped mass attached to the two facesheets, as shown in Fig. 2. Due to periodicity, a unit cell of the sandwich structure is shown in Fig. 3(a), whereas its equivalent structure is presented in Fig. 3(b). For simplicity, the facesheets and the core are both made of aluminum, and have geometrical and material properties as follows: core thickness t_0 and depth l, panel thickness h_1 and h_2 (subscripts "1" and "2" denote left- and right-side facesheets, respectively), unit cell length L, inclination angle between panel and core sheet $\pm\alpha$, Young's modulus E, and Poisson ratio ν.

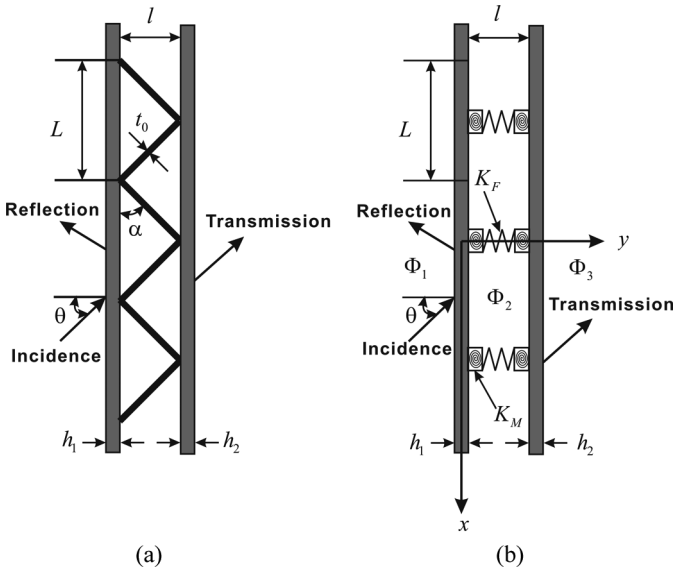

FIGURE 2.—(a) Side view of sandwich panel with corrugated core. (b) Schematic of equivalent structure for space-harmonic modeling [13, 23].

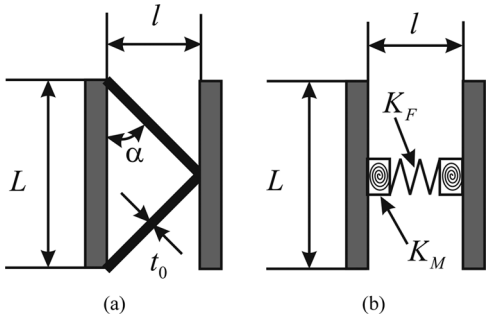

FIGURE 3.—(a) Unit cell of sandwich panel with corrugated core. (b) Equivalent unit cell [13, 23].

With the assumption of small deflections, the stiffness of the translational spring K_F and the stiffness of the rotational spring K_M per unit length can be obtained analytically (details can be found in Xin et al. [13]). Let the surface density of the left- and right-side facesheets be denoted by m_1 and m_2, respectively. The mass of the core for one unit cell is $2M$, which is equivalent to two lumped mass M separately attached to the inner surfaces of the two facesheets [Fig. 3(b)]. Under these conditions, the governing equations for the vibration of the sandwich structure may be written as [13, 23]:

$$D_1\frac{\partial^4 w_1(x,t)}{\partial x^4}+\left(m_1+\frac{M}{L}\right)\frac{\partial^2 w_1(x,t)}{\partial t^2}+K_F(w_1(x,t)-w_2(x,t))-K_M\frac{\partial^2}{\partial x^2}(w_1(x,t)-w_2(x,t))-j\omega\rho_0(\Phi_1-\Phi_2)=0, \quad (1)$$

$$D_2\frac{\partial^4 w_2(x,t)}{\partial x^4}+\left(m_2+\frac{M}{L}\right)\frac{\partial^2 w_2(x,t)}{\partial t^2}+K_F(w_2(x,t)-w_1(x,t))-K_M\frac{\partial^2}{\partial x^2}(w_2(x,t)-w_1(x,t))-j\omega\rho_0(\Phi_2-\Phi_3)=0, \quad (2)$$

where ρ_0 is air density, w_i $(i=1,2)$ are the transverse deflections of the two facesheets, $j=\sqrt{-1}$, and Φ_i $(i=1,2,3)$ is the velocity potential of the acoustic field [see Fig. 2(b)] which is related to the corresponding velocity by $\hat{u}_i=-\nabla\Phi_i$. With the loss factor of facesheet material denoted by η_i, the flexural rigidity of the facesheet D_i $(i=1,2)$ can be written using complex Young's modulus $E_i(1+j\eta_i)$, as

$$D_i=\frac{E_i h_i^3(1+j\eta_i)}{12(1-v_i^2)}. \quad (3)$$

The velocity potentials of acoustic fields, i.e., the incident field, the air cavity field in between the two facesheets, and the transmitted field [Fig. 2(b)] are separately defined as follows [13, 23, 42]:

$$\Phi_1(x,y,t)=Ie^{-j\left[k_x x+k_y y-\omega t\right]}+\sum_{-\infty}^{\infty}\beta_n e^{-j\left[(k_x+2n\pi/L)x-k_{yn}y-\omega t\right]}, \quad (4)$$

$$\Phi_2(x,y,t)=\sum_{-\infty}^{\infty}\varepsilon_n e^{-j\left[(k_x+2n\pi/L)x+k_{yn}y-\omega t\right]}+\sum_{-\infty}^{\infty}\zeta_n e^{-j\left[(k_x+2n\pi/L)x-k_{yn}y-\omega t\right]}, \quad (5)$$

$$\Phi_3(x,y,t)=\sum_{-\infty}^{\infty}\xi_n e^{-j\left[(k_x+2n\pi/L)x+k_{yn}y-\omega t\right]}, \quad (6)$$

where I and β_n are the amplitudes of the incident (i.e., positive-going) sound wave and the reflected (i.e., negative-going) sound wave, respectively. Similarly, symbols ε_n and ζ_n represent separately the amplitude of the positive-going wave and the negative-going wave in the air cavity field. In the transmitted field, there is no negative-going waves, thus the velocity potential is only for transmitted wave with amplitude ξ_n.

The wavenumbers k_x and k_y appear in Eqs. (4) to (6) are determined by sound incidence angle θ, as

$$k_x=k\sin\theta,\quad k_y=k\cos\theta, \quad (7)$$

where $k=\omega/c_0$, c_0 is sound speed in air, and k_{yn} is the wavenumber in the y-direction, defined as [13]

$$k_{yn}=\sqrt{\left(\frac{\omega}{c}\right)^2-\left(k_x+\frac{2n\pi}{L}\right)^2}, \quad (8)$$

when $\omega/c<|k_x+2n\pi/L|$, the pressure waves become evanescent waves and, correspondingly, k_{yn} is given by

$$k_{yn}=j\sqrt{\left(k_x+\frac{2n\pi}{L}\right)^2-\left(\frac{\omega}{c}\right)^2}. \quad (9)$$

For harmonic sound excitations of the infinitely large and periodic sandwich structure, the deflections of the two facesheets can be expressed as [13, 42]

$$w_1(x,t)=\sum_{n=-\infty}^{\infty}\alpha_{1,n}e^{-j[k_x+2n\pi/L]x}e^{j\omega t}, \quad (10)$$

$$w_2(x,t)=\sum_{n=-\infty}^{\infty}\alpha_{2,n}e^{-j[k_x+2n\pi/L]x}e^{j\omega t}. \quad (11)$$

At the interface of the air and the facesheet, the continuity of velocity should be satisfied, i.e., the normal velocity of the facesheet matches with that of its adjacent air particle:

$$-\frac{\partial\Phi_1}{\partial z}=j\omega w_1,\quad -\frac{\partial\Phi_2}{\partial z}=j\omega w_1;\quad \text{at } y=0, \quad (12)$$

$$-\frac{\partial\Phi_2}{\partial z}=j\omega w_2,\quad -\frac{\partial\Phi_3}{\partial z}=j\omega w_2;\quad \text{at } y=H. \quad (13)$$

Substitution of Eqs. (4) to (6), Eqs. (10) and (11) into Eqs. (12) and (13) leads to

$$\beta_0=I-\omega\alpha_{1,0}/k_y, \quad (14)$$

$$\beta_n=-\omega\alpha_{1,n}/k_{yn},\quad \text{when } n\neq 0, \quad (15)$$

$$\varepsilon_n=\frac{\omega\left(\alpha_{2,n}e^{jk_{yn}H}-\alpha_{1,n}e^{2jk_{yn}H}\right)}{k_{yn}\left(1-e^{2jk_{yn}H}\right)}, \quad (16)$$

$$\zeta_n=\frac{\omega\left(\alpha_{2,n}e^{jk_{yn}H}-\alpha_{1,n}\right)}{k_{yn}\left(1-e^{2jk_{yn}H}\right)}, \quad (17)$$

$$\xi_n=\omega\alpha_{2,n}e^{jk_{yn}H}/k_{yn}. \quad (18)$$

Substituting Eqs. (4) to (6), Eqs. (10) and (11) into the governing equations, and incorporating Eqs. (14) to (18), one obtains [13]

$$\left[D_1\left(k_x+\frac{2m\pi}{L}\right)^4-m_1\omega^2-\frac{2j\omega^2\rho_0 e^{jk_{ym}H}}{k_{ym}\left(1-e^{2jk_{ym}H}\right)}\right]\alpha_{1,m}+\frac{K_t-\omega^2 M}{L}\left(\sum_{n=-\infty}^{\infty}\alpha_{1,n}\right)+\frac{K_r}{L}\left[\sum_{n=-\infty}^{\infty}\alpha_{1,n}\left(k_x+\frac{2n\pi}{L}\right)\right]\left(k_x+\frac{2m\pi}{L}\right)-\frac{K_t}{L}\left(\sum_{n=-\infty}^{\infty}\alpha_{2,n}\right)-\frac{K_r}{L}\left[\sum_{n=-\infty}^{\infty}\alpha_{2,n}\left(k_x+\frac{2n\pi}{L}\right)\right]$$

$$\times \left(k_x + \frac{2m\pi}{L}\right) + \frac{2j\omega^2\rho_0 e^{jk_{yn}H}}{k_{yn}\left(1 - e^{2jk_{yn}H}\right)}\alpha_{2,m} = \begin{cases} 2j\omega^2\rho_0 I, & m = 0 \\ 0, & m \neq 0 \end{cases} \quad (19)$$

$$\left[D_2\left(k_x + \frac{2m\pi}{L}\right)^4 - m_2\omega^2 - \frac{2j\omega^2\rho_0 e^{jk_{yn}H}}{k_{yn}\left(1 - e^{2jk_{yn}H}\right)}\right]\alpha_{2,m} + \frac{K_t - \omega^2 M}{L}\left(\sum_{n=-\infty}^{\infty}\alpha_{2,n}\right) + \frac{K_r}{L}\left[\sum_{n=-\infty}^{\infty}\alpha_{2,n}\left(k_x + \frac{2n\pi}{L}\right)\right] \times \left(k_x + \frac{2m\pi}{L}\right) - \frac{K_t}{L}\left(\sum_{n=-\infty}^{\infty}\alpha_{1,n}\right) - \frac{K_r}{L}\left[\sum_{n=-\infty}^{\infty}\alpha_{1,n}\left(k_x + \frac{2n\pi}{L}\right)\right]\left(k_x + \frac{2m\pi}{L}\right) + \frac{2j\omega^2\rho_0 e^{jk_{yn}H}}{k_{yn}\left(1 - e^{2jk_{yn}H}\right)}\alpha_{1,m} = 0 \quad (20)$$

where the unknown coefficients $\alpha_{1,n}$ and $\alpha_{2,n}$ can be obtained by simultaneously solving the above algebraic equations. Once these coefficients are known, parameters β_n, ε_n, ζ_n, ξ_n can be obtained by applying Eqs. (14) to (18).

Finally, the power transmission coefficient is defined as the ratio of incident sound power to transmitted sound power [13, 23], as

$$\tau(\theta) = \frac{\sum_{n=-\infty}^{\infty}|\xi_n|^2 Re\left(k_{yn}\right)}{|I|^2 k_y}. \quad (21)$$

Correspondingly, the sound transmission loss (*STL*) is defined in decibel scale as

$$STL = -10\log_{10}\tau. \quad (22)$$

Numerical results and discussions

Numerical simulations are performed in this section to investigate the effects of core topology (determined by inclination angle α between facesheet and core sheet) on the sound insulation performance of an all-metallic sandwich panel with corrugated core. In the subsequent analysis of the core topology effects on STL (i.e., Section 3.1) and optimal design (i.e., Section 3.3), the two sound transmission routes (i.e., airborne route and structure-borne route) are both considered, just as the theoretical model previously derived. However, to avoid the singularity problem in mathematics, the physical interpretations for the existence of peaks and dips in STL curves in Section 3.2 neglect the airborne route of sound transmission and only consider the predominant structural route, so that a clear understanding of the peaks and dips can be obtained. The structural dimensions and material properties of the panel used in the numerical investigations are presented in Table 1.

Table 1.—Structural dimensions and material properties.

Descriptions	Values
Material properties (aluminum)	
Young's modulus	$E = 70\,\text{GPa}$
Density	$\rho = 2700\,\text{kg/m}^3$
Poisson ratio	$\nu = 0.33$
Loss factor	$\eta = 0.01$
Air properties	
Density	$\rho_0 = 1.21\,\text{kg/m}^3$
Sound speed	$c_0 = 343\,\text{m/s}$
Structural dimensions	
Core depth	$l = 21.5\,\text{mm}$
Core sheet thickness	$t_0 = 1\,\text{mm}$
Facesheet thickness	$h_1 = h_2 = 2\,\text{mm}$

Effects of Core Topology on Sound Transmission Across the Sandwich Structure

To highlight the effects of core topology on sound transmission across the sandwich structure, the inclination angle α is systematically varied while all other parameters are held constant. The *STL* values numerically calculated with the space-harmonic method are plotted as functions of frequency in Fig. 4 for selected values of α: 20°, 30°, 45°, and 60°. Due to the similar qualitative aspect of the STL versus frequency curves for different incidence angles [39] and for the purpose of sufficiently exciting the structural vibration modes, the sound incident angle is fixed at $\theta = 45°$.

At frequencies corresponding separately to the "mass-air-mass" resonance, the standing-wave resonance, the "coincidence" resonance, and the structure natural resonance, the sandwich structure vibrates intensely. This significantly decreases the sound insulation capability of the structure, resulting in the existence of various dips in Fig. 4. The "mass-air-mass" resonance appears in the process of sound transmission through a "panel-air-panel" type structure, at which the two panels move in opposite phase, with the air in between bouncing like springs. This resonance is active only when the frequency of the incident sound matches the natural frequency of the "mass-air-mass" resonance. Similarly, the acoustic standing-wave resonance is also a feature of the "panel-air-panel" type structure, which occurs when the air cavity depth is integer numbers of the half-wavelengths of incident sound. The "coincidence" frequency is relevant to the condition that the trace wavelength of the incidence sound matches the wavelength of bending wave in the facesheet. For the sandwich panel considered here, when sound is normally incident, the mass-air-mass resonance occurs at around 280 Hz, the first order standing wave resonance occurs at about 8000 Hz, while the critical frequency beyond which the coincident resonance will occur is around 6000 Hz (in comparison, the coincidence frequency is about 12000 Hz for a typical sound incidence with angle $\theta = 45°$). In addition, due to the complexity and periodicity of the sandwich structure as well as fluid-structural coupling, the "mass-air-mass" resonance, the standing-wave resonance,

the "coincidence" and the structure natural resonance are mutually coupled, creating a series of peaks and dips on the *STL* curves as shown in Fig. 4. A more detailed physical interpretation for the existence of those peaks and dips in structure-borne STL curves which are associated with the structure natural resonance only is presented in the next section.

It can be seen from Fig. 4 that the geometry of the corrugated core plays a significant role in the process of sound transmission through the sandwich. As the inclination angle is increased, not only the peaks and dips of the *STL* versus frequency curve are all shifted to higher frequencies, but also the smooth range of the curve at lower frequencies is stretched towards higher frequencies. The primary reason is that the change of inclination angle alters the equivalent stiffness of the translational and rotational springs as well as the unit cell length (see Xin et al. [13]), and hence the vibroacoustic behavior of the whole sandwich structure is changed. In other words, the sandwich structure with corrugated core can be regarded as a structure with inherent vibroacoustic properties that can be favorably altered by tuning its core geometry in terms of factual application requirements.

Physical Interpretation for the Existence of Peaks and Dips on STL Curves

The corrugated core in-between the two facesheets stiffens the sandwich structure for enhanced load bearing capability. However, its existence adds one structural route for sound propagation, resulting in the decrease of *STL* and the intense peaks and dips on *STL* versus frequency curves relative to double-leaf panel structures with air cavity. These peaks and dips caused by the core geometry as well as periodicity of the sandwich structure have a significant effect on its sound insulation performance, so it is necessary to explore their physical origins.

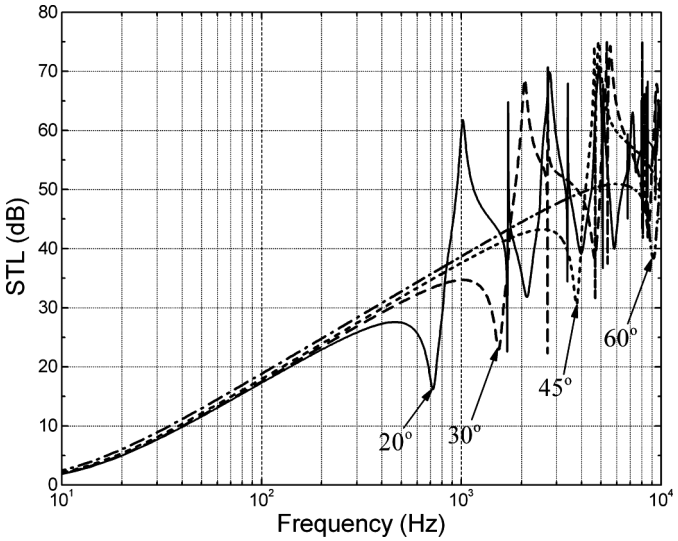

FIGURE 4.—*STL* of sandwich panels with different inclination angles (as shown in Fig. 2) in the case of incidence angle $\theta = 45°$.

As mentioned above, the appearance of dips on *STL* curves is attributed to the effects of vibroacoustic resonances, the most likely being the familiar "coincidence" resonance discussed in the previous section. Whilst the bending waves induced by the incident sound transmit in the facesheet, the reflected waves from the core sheets also act on the facesheet, which thence generate multiple possibilities for the wavenumbers of the two waves matching and coinciding with each other. To emphasize the main effects and investigate how the "fake coincidence resonances" affect *STL* curves, material damping is ignored here, and only the panel-core-panel route for wave transmission is considered. Furthermore, for simplicity, the coupling effects of air cavity between the two facesheets are ignored, and the mass and the equivalent rotational stiffness of the corrugated core are not taken into account. These assumptions are generally reasonable inasmuch as the structural coupling of the corrugated core is much stronger than the acoustic coupling of air cavity and the rotational stiffness of the core has a negligible effect with respect to its translational stiffness. The governing equations for facesheet vibration can, therefore, be simplified as

$$D_1\frac{\partial^4 w_1(x,t)}{\partial x^4} + m_1\frac{\partial^2 w_1(x,t)}{\partial t^2} + K_F(w_1(x,t) - w_2(x,t)) = 0, \tag{23}$$

$$D_2\frac{\partial^4 w_2(x,t)}{\partial x^4} + m_2\frac{\partial^2 w_2(x,t)}{\partial t^2} + K_F(w_2(x,t) - w_1(x,t)) = 0. \tag{24}$$

As shown in Fig. 2(b), the equivalent of the sandwich structure with corrugated core is a symmetrical construction. The transmission of bending wave in the structure can be divided into two parts. One is the symmetrical vibration of the construction, in which the two facesheets move in opposite phase, both in or both out at the same time, analogous to the "breathing" motion of animals. Here, the corrugated core has a strong constraint influence on the two facesheets. The other is antisymmetric motion, in which the structure vibrates in step (the two facesheets move in the same phase) with the core carried by the facesheets. In this case, the core exerts no constraint on the movement of the facesheets. In other words, the sandwich structure vibrating in antisymmetric motion can be considered as a single panel in movement.

As for the antisymmetric motion, it can be observed that its dispersion curve [dash-dot line shown in Fig. 5(a)] is a continuous parabola, so sinusoidal vibration waves with any frequency can transmit along the length direction in the sandwich panel. While the periodic corrugated core in-between the facesheets has a significant effect on the dispersion relation of the construction for symmetrical motion, whose dispersion curves (calculated with the transfer matrix method proposed by Mead [24]) consist of a series of periodic distributions of "pass-band" and "stop-band." At the frequency range corresponding to the "pass-band," for a given frequency there exist infinite wavenumbers that are relevant to this frequency: the

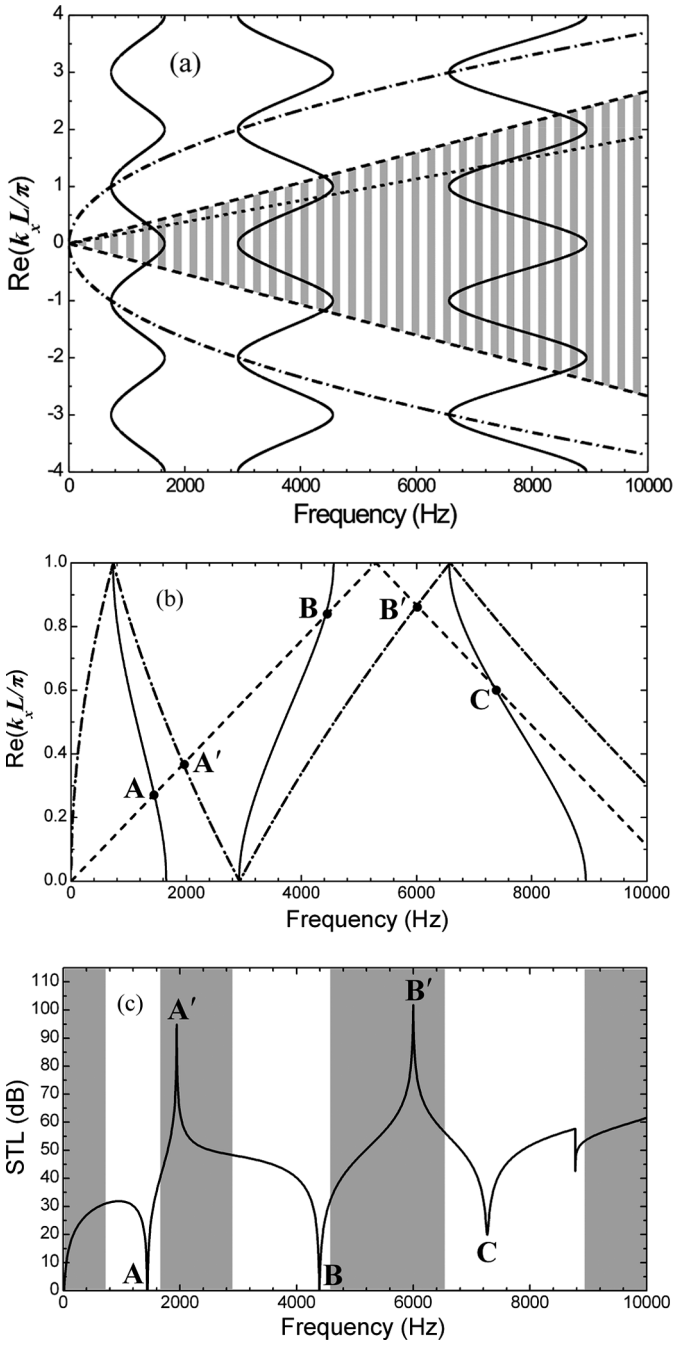

FIGURE 5.—(a) Normalized wavenumber versus frequency. Solid line: "pass-band" of symmetrical motion; dash-dot line: dispersion curve of antisymmetric motion; dash line: dispersion curve corresponding to incident sound at $\theta = \pm 90°$, with the wedge bounded in between the two lines called sound radiation area; short dash line: dispersion curve corresponding to incident sound at $\theta = 45°$. (b) Real part of normalized wavenumber versus frequency curve [i.e., "folding" version of Fig. 5(a)]. Solid line: dispersion curve of symmetrical motion; dash-dot line: dispersion curve of antisymmetric motion; dash line: dispersion curve corresponding to incident sound at $\theta = 90°$; short dash line: dispersion curve corresponding to incident sound at $\theta = 45°$. (c) Relevant *STL* curve. Shading area: "stop-band"; blank area: "pass-band".

traveling wave identified by the correlative frequency and wavenumber can transmit along the length direction in the structure without any attenuation. Whereas, in the areas of "stop-band," there is no wavenumber relevant to a given frequency: the bending waves transmitting in the structure with these frequencies are quickly evanescent in exponent form along the length direction in the structure. These "pass-bands" and "stop-bands" are primary responsible for the appearances of peaks and dips on the *STL* versus frequency curves shown in Fig. 4.

Note that the short dash line in Fig. 5(a) represents the dispersion relation for incident sound with angle $\theta = 45°$ and two dash lines represent the dispersion curve for incidence sound with angle $\theta = \pm 90°$, respectively. Thus the wedge bounded in between the two lines is the frequency/wavenumber area in which a wave in the sandwich structure can radiate sound.

It can be observed from Fig. 5(a) that there is no intersection between the dispersion curve of antisymmetric motion and the sound radiation area, implying that the antisymmetric motion caused by the incident sound cannot reach enough intensity to radiate sound waves except at the coincidence frequency. For the symmetrical motion of the sandwich, however, there are intersections of the dispersion curve for sound wave with a certain incidence angle, one per pass band. At the frequencies corresponding to these intersections, the incident sound can excite structure vibration strong enough to radiate sound, causing the appearance of *STL* dips, as shown in Figs. 5(b) and (c). Actually, Fig. 5(b) is the "folding" version of Fig. 5(a) in the range from 0 to 1. As a compact diagram, this fold manipulation is often employed in theoretical studies of sound propagation across periodic structures [23]. The *STL* versus frequency curve of the simplified problem (in which the mass and rotational stiffness of the core as well as air cavity coupling effects are all ignored) is presented in Fig. 5(c) using the same frequency scale as Figs. 5(a) and (b). It can be readily seen that the intersections labeled by A, B, and C in Fig. 5(b) correspond with the *STL* dips labeled by the same symbols in Fig. 5(c).

The intersections labeled by A' and B' in Fig. 5(b) are closely related to the two steep peaks in Fig. 5(c). With reference to Fig. 5(a), the intersections A' and B' do not really exist, whose appearances are owing to the "folding" manipulation from Fig. 5(a) to Fig. 5(b). However, at the frequencies corresponding to these intersections, the transverse deflection of the vibratory facesheet only takes two terms in Eq. (10): one for the driven term $n = 0$, and the other in accord with the resonance condition [obtained from Eq. (23)] of the driven facesheet [42]:

$$D_1 (k_x + 2N\pi/L)^4 - m_1\omega^2 = 0. \tag{25}$$

The transverse deflection of the facesheet is a summation of these two terms, namely,

$$W_1 = Ij\omega\rho_0 e^{-j(k_x x - \omega t)} \left[\frac{1 - e^{-j2N\pi x/L}}{D_1 k_x^4 - m_1\omega^2} \right]. \tag{26}$$

It can be obtained from Eq. (26) that the joints which connect the equivalent springs and the driven facesheet are

just the nodal points of standing wave in the facesheet. Consequently, the joints have no displacement and the springs do not transfer any force to the other facesheet. As a result, there is no sound radiation because the radiating facesheet is stationary without any movement. Naturally, at these frequencies relevant to the "fake" interactions in Fig. 5(b), the sharp peaks on the *STL* curve will occur.

Optimal Design for Combined Sound Insulation and Structural Load Capacity

It has thus far been demonstrated that core topology play a significant role in the sound insulation performance of the sandwich structure. Similarly, the structural load capacity of the sandwich is also strongly dependent upon the core geometry [1, 58]. It is therefore of interest to investigate the role of core geometry when the acoustic and structural properties of the sandwich structure are considered simultaneously. To this end, several dimensionless parameters are introduced.

The first dimensionless parameter introduced is the normalized mass of the sandwich (i.e., ratio of the mass of one unit cell to that of the solid filling the whole volume of the unit cell):

$$\bar{m} = \frac{(h_1 + h_2)\, L + 2lt_0/\sin\alpha}{L\,(l + h_1 + h_2)}. \tag{27}$$

As the core for a load-bearing sandwich panel, the in-plane shear modulus is the most important, due to the fact that upon loading the panel deflects as a result of combined bending and shear deformation [1]. The in-plane shear modulus G of the corrugated core can be calculated following Eq. (35) in Ref. [58], and normalized as

$$\widetilde{G} = \frac{G}{E}. \tag{28}$$

Together with the above defined dimensionless parameters and the sound insulation index *STL*, an integrated index for optimal design towards a lightweight sandwich with superior load-bearing and sound isolation properties may be defined as

$$\gamma_{SGM} = \frac{STL \times \widetilde{G}}{\tilde{m}}. \tag{29}$$

Note that *STL*, $\widetilde{G}$, and $\tilde{m}$ are all functions of inclination angle α of the corrugated core.

Figure 6 plots γ_{SGM} as a function of frequency for selected core inclination angles (20°, 30°, 45°, 60°, and 70°), with the sound incidence angle fixed at $\theta = 45°$. It is seen from Fig. 6 that when the inclination angle α is smaller than 45°, the index γ_{SGM} increases with the increase of α, whereas in the range of $45° < \alpha < 60°$ the index γ_{SGM} maintains the same value over a wide frequency range, except for discrepancies at frequencies higher than 3×10^3 Hz. As the inclination angle is increased beyond 60°, the magnitude of γ_{SGM} decreases. Note that the higher the index γ_{SGM} is, the more superior of the combined acoustic and structural performance of the sandwich will be. Therefore, it can be concluded from Fig. 6 that a core inclination angle in the range of 45° to 60° is the preferred selection for the sandwich structure.

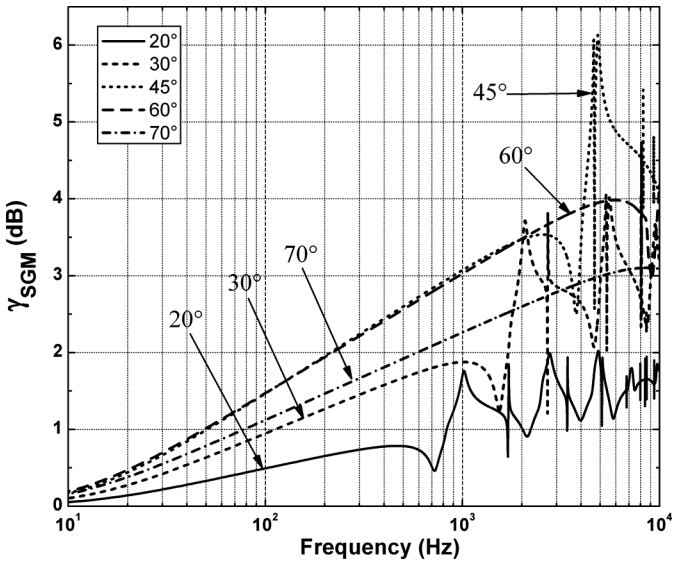

FIGURE 6.—Tendency plot of γ_{SGM} versus frequency for selected core inclination angles (as shown in Fig. 2) for fixed sound incidence angle of $\theta = 45°$.

CONCLUSION

The influence of the core topology on the sound insulation capability of a two-dimensional periodic sandwich configuration with corrugated core is theoretically analyzed by the space-harmonic method. In the theoretical model, an equivalent structure containing one translational spring and one rotational spring per unit cell is proposed to simplify the analysis of the vibroacoustic problem. Obtained results demonstrate that the core topology significantly influences the sound insulation performance of the structure, so that one may tailor the core topology for specified acoustic applications. Subsequent analysis of the *STL* and dispersion curves of the sandwich structure leads to fundamental insight into the physical mechanisms behind the appearances of various peaks and dips on the *STL* curves.

As the inclination angle between the facesheet and the core sheet is increased, the peaks and dips on *STL* curves are shifted towards higher frequencies, the *STL* values increase on the whole, while the smooth portion of the *STL* curve in low frequencies is stretched longer.

For a given incident sound angle, the *STL* dips occur at frequencies corresponding to the interactions between the dispersion curve and the symmetrical motion of the structure. The peaks on *STL* occur because the junctions which connect the equivalent springs and the driven facesheet are just the nodal points of the standing bending wave traveling in the incident facesheet.

As the weight, stiffness, and acoustic property of the sandwich structures all change with the alteration of core configuration and geometry, it is possible to explore the

multifunctionality of the structure by optimally designing the core topology.

Acknowledgments

This work is supported by the National Basic Research Program of China (2011CB610300), the National 111 Project of China (B06024), the National Natural Science Foundation of China (11072188 and 10825210), the Shaanxi Province 13115 project (52010ZDKG704) and the Fundamental Research Funds for the Central Universities.

References

1. Gu, S.; Lu, T.J.; Evans, A.G. On the design of two-dimensional cellular metals for combined heat dissipation and structural load capacity. Int. J. Heat Mass Transfer **2001**, *44* (11), 2163–2175.
2. Lu, T.J.; Chen, C.; Zhu, G. Compressive behaviour of corrugated board panels. J. Comp. Mater. **2001**, *35* (23), 2098–2126.
3. Franco, F.; Cunefare, K.A.; Ruzzene, M. Structural-acoustic optimization of sandwich panels. ASME J. Vib. Acoust. **2007**, *129* (3), 330–340.
4. Spadoni, A.; Ruzzene, M. Structural and acoustic behavior of chiral truss-core beams. ASME J. Vib. Acoust. **2006**, *128* (5), 616–626.
5. Wu, S.F.; Wu, G.; Puskarz, M.M.; Gleason, M.E. Noise transmission through a vehicle side window due to turbulent boundary layer excitation. J. Vib. Acoust. **1997**, *119* (4), 557–562.
6. Xin, F.X.; Lu, T.J.; Chen, C.Q. External mean flow influence on noise transmission through double-leaf aeroelastic plates. AIAA J. **2009**, *47* (8), 1939–1951.
7. Carneal, J.P.; Fuller, C.R. An analytical and experimental investigation of active structural acoustic control of noise transmission through double panel systems. J. Sound Vib. **2004**, *272* (3–5), 749–771.
8. Grosveld, F. Plate acceleration and sound transmission due to random acoustic and boundary-layer excitation. AIAA J. **1992**, *30* (3), 601–607.
9. Xin, F.X.; Lu, T.J.; Chen, C.Q. Dynamic response and acoustic radiation of double-leaf metallic panel partition under sound excitation. Comp. Mater. Sci. **2009**, *46* (3), 728–732.
10. Maury, C.; Gardonio, P.; Elliott, S.J. Model for active control of flow-induced noise transmitted through double partitions. AIAA J. **2002**, *40* (6), 1113–1121.
11. Thamburaj, P.; Sun, J.Q. Effect of material and geometry on the sound and vibration transmission across a sandwich beam. ASME J. Vib. Acoust. **2001**, *123* (2), 205–212.
12. Lyle, K.; Mixson, J. Laboratory study of sidewall noise transmission and treatment for a light aircraft fuselage. J. Aircr. **1987**, *24* (9), 660–665.
13. Xin, F.X.; Lu, T.J.; Chen, C.Q. Sound transmission across lightweight all-metallic sandwich panels with corrugated cores. Chin. J. Acoust. **2009**, *28* (3), 231–243.
14. Xin, F.X.; Lu, T.J.; Chen, C.Q. Sound transmission through simply supported finite double-panel partitions with enclosed air cavity. ASME J. Vib. Acoust. **2010**, *132* (1), 011008.
15. Xin, F.X.; Lu, T.J. Analytical modeling of fluid loaded orthogonally rib-stiffened sandwich structures: Sound transmission. J. Mech. Phys. Solids. **2010**, *58* (9), 1374–1396.
16. Xin, F.X.; Lu, T.J. Analytical modeling of sound transmission across finite aeroelastic panels in convected fluids. J. Acoust. Soc. Am. **2010**, *128* (3), 1097–1107.
17. Xin, F.X.; Lu, T.J. Analytical modeling of sound transmission through clamped triple-panel partition separated by enclosed air cavities. Eur. J. Mech. A-Solid **2011**, *30* (6), 770–782.
18. Xin, F.X.; Lu, T.J. Transmission loss of orthogonally rib-stiffened double-panel structures with cavity absorption. J. Acoust. Soc. Am. **2011**, *129* (4), 1919–1934.
19. Xin, F.X.; Lu, T.J. Analytical modeling of wave propagation in orthogonally rib-stiffened sandwich structures: Sound radiation. Comput. Struct. **2011**, *89* (5–6), 507–516.
20. Xin, F.X.; Lu, T.J. Sound radiation of orthogonally rib-stiffened sandwich structures with cavity absorption. Compos. Sci. Technol. **2010**, *70* (15), 2198–2206.
21. Lu, T.J.; Valdevit, L.; Evans, A.G. Active cooling by metallic sandwich structures with periodic cores. Progress in Materials Science **2005**, *50* (7), 789–815.
22. Liu, T.; Deng, Z.C.; Lu, T.J. Bi-functional optimization of actively cooled, pressurized hollow sandwich cylinders with prismatic cores. Journal of the Mechanics and Physics of Solids **2007**, *55* (12), 2565–2602.
23. Xin, F.X.; Lu, T.J.; Chen, C. Sound transmission through lightweight all-metallic sandwich panels with corrugated cores. Adv. Mater. Res. **2008**, *47–50*, 57–60.
24. Mead, D.J. Free wave propagation in periodically supported, infinite beams. J. Sound Vib. **1970**, *11* (2), 181–197.
25. Mead, D.J.; Pujara, K.K. Space-harmonic analysis of periodically supported beams: Response to convected random loading. J. Sound Vib. **1971**, *14* (4), 525–532.
26. Lomas, N.S.; Hayek, S.I. Vibration and acoustic radiation of elastically supported rectangular plates. J. Sound Vib. **1977**, *52* (1), 1–25.
27. Renji, K. Sound transmission loss of unbounded panels in bending vibration considering transverse shear deformation. J. Sound Vib. **2005**, *283* (1–2), 478–486.
28. Sewell, E.C. Transmission of reverberant sound through a single-leaf partition surrounded by an infinite rigid baffle. J. Sound Vib. **1970**, *12*(1), 21–32.
29. Cummings, A.; Mulholland, K.A. The transmission loss of finite sized double panels in a random incidence sound field. J. Sound Vib. **1968**, *8* (1), 126–133.
30. Mulholland, K.A.; Parbrook, H.D.; Cummings, A. The transmission loss of double panels. J. Sound Vib. **1967**, *6* (3), 324–334.
31. Beranek, L.L.; Work, G.A. Sound transmission through multiple structures containing flexible blankets. J. Acoust. Soc. Am. **1949**, *21* (4), 419–428.
32. London, A. Transmission of reverberant sound through double walls. J. Acoust. Soc. Am. **1950**, *22* (2), 270–279.
33. Sewell, E.C. Two-dimensional solution for transmission of reverberant sound through a double partition. J. Sound Vib. **1970**, *12* (1), 33–57.
34. White, P.H.; Powell, A. Transmission of random sound and vibration through a rectangular double wall. J. Acoust. Soc. Am. **1966**, *40* (4), 821–832.
35. Hongisto, V. Sound insulation of doors—Part 1: Prediction models for structural and leak transmission. J. Sound Vib. **2000**, *230* (1), 133–148.
36. Chazot, J.D.; Guyader, J.L. Prediction of transmission loss of double panels with a patch-mobility method. J. Acoust. Soc. Am. **2007**, *121*(1), 267–278.

37. Xin, F.X.; Lu, T.J.; Chen, C.Q. Vibroacoustic behavior of clamp mounted double-panel partition with enclosure air cavity. J. Acoust. Soc. Am. **2008**, *124*(6), 3604–3612.
38. Xin, F.X.; Lu, T.J. Analytical and experimental investigation on transmission loss of clamped double panels: Implication of boundary effects. J. Acoust. Soc. Am. **2009**, *125* (3), 1506–1517.
39. Lee, J.H.; Kim, J. Analysis of sound transmission through periodically stiffened panels by space-harmonic expansion method. J. Sound Vib. **2002**, *251* (2), 349–366.
40. Lin, G.-F.; Garrelick, J.M. Sound transmission through periodically framed parallel plates. J. Acoust. Soc. Am. **1977**, *61* (4), 1014–1018.
41. Takahashi, D. Sound radiation from periodically connected double-plate structures. J. Sound Vib. **1983**, *90* (4), 541–557.
42. Wang, J.; Lu, T.J.; Woodhouse, J.; Langley, R.S.; Evans, J. Sound transmission through lightweight double-leaf partitions: Theoretical modelling. J. Sound Vib. **2005**, *286* (4–5), 817–847.
43. El-Raheb, M.; Wagner, P. Effects of end cap and aspect ratio on transmission of sound across a truss-like periodic double panel. J. Sound Vib. **2002**, *250* (2), 299–322.
44. Lauriks, W.; Mees, P.; Allard, J.F. The acoustic transmission through layered systems. J. Sound Vib. **1992**, *155* (1), 125–132.
45. Trochidis, A.; Kalaroutis, A. Sound transmission through double partitions with cavity absorption. J. Sound Vib. **1986**, *107* (2), 321–327.
46. Narayanan, S.; Shanbhag, R.L. Sound transmission through a damped sandwich panel. J. Sound Vib. **1982**, *80* (3), 315–327.
47. Nilsson, A.C. Wave propagation in and sound transmission through sandwich plates. J. Sound Vib. **1990**, *138* (1), 73–94.
48. Ford, R.D.; Lord, P.; Walker, A.W. Sound transmission through sandwich constructions. J. Sound Vib. **1967**, *5* (1), 9–21.
49. Nilsson, A.C. Some acoustical properties of floating-floor constructions. J. Acoust. Soc. Am. **1977**, *61* (6), 1533–1539.
50. Narayanan, S.; Shanbhag, R.L. Sound transmission through elastically supported sandwich panels into a rectangular enclosure. J. Sound Vib. **1981**, *77* (2), 251–270.
51. Huang, W.C.; Ng, C.F. Sound insulation improvement using honeycomb sandwich panels. Appl. Acoust. **1998**, *53* (1–3), 163–177.
52. Foin, O.; Nicolas, J.; Atalla, N. An efficient tool for predicting the structural acoustic and vibration response of sandwich plates in light or heavy fluid. Appl. Acoust. **1999**, *57*, 213–242.
53. Wang, T.A.; Sokolinsky, V.S.; Rajaram, S.; Nutt, S.R. Assessment of sandwich models for the prediction of sound transmission loss in unidirectional sandwich panels. Appl. Acoust. **2005**, *66* (3), 245–262.
54. Ng, C.F.; Hui, C.K. Low frequency sound insulation using stiffness control with honeycomb panels. Appl. Acoust. **2008**, *69* (4), 293–301.
55. Cordonnier-Cloarec, P.; Pauzin, S.; Biron, D.; Haddar, M.; Hamdi, M.A. Contribution to the study of sound transmission and radiation of corrugated steel structures. J. Sound Vib. **1992**, *157* (3), 515–530.
56. Ng, C.F.; Zheng, H. Sound transmission through double-leaf corrugated panel constructions. Appl. Acoust. **1998**, *53* (1–3), 15–34.
57. Mathur, G.P. Sound transmission through stiffened double-panel structures lined with elastic porous materials. In *Proceedings of the 14th DGLR/AIAA Aero-Acoustics Conference*, Aachen, Germany, May 11–14, 1992; 102–105.
58. Liu, T.; Deng, Z.; Lu, T. Structural modeling of sandwich structures with lightweight cellular cores. Acta Mech. Sinica. **2007**, *23* (5), 545–559.